nature structural & molecular biology

Structural basis for ATP-dependent DnaA assembly and replication-origin remodeling

Jan P Erzberger, Melissa L Mott & James M Berger

In bacteria, the initiation of replication is controlled by DnaA, a member of the ATPases associated with various cellular activities (AAA+) protein superfamily. ATP binding allows DnaA to transition from a monomeric state into a large oligomeric complex that remodels replication origins, triggers duplex melting and facilitates replisome assembly. The crystal structure of AMP-PCP–bound DnaA reveals a right-handed superhelix defined by specific protein-ATP interactions. The observed quaternary structure of DnaA, along with topology footprint assays, indicates that a right-handed DNA wrap is formed around the initiation nucleoprotein complex. This model clarifies how DnaA engages and unwinds bacterial origins and suggests that additional, regulatory AAA+ proteins engage DnaA at filament ends. Eukaryotic and archaeal initiators also have the structural elements that promote open-helix formation, indicating that a spiral, open-ring AAA+ assembly forms the core element of initiators in all domains of life.

Initiators are *trans*-acting protein factors that help remodel DNA superstructure at replication origins to enable replisome assembly[1]. Cellular initiators, which include monomeric prokaryotic proteins and the multisubunit eukaryotic origin recognition complex (ORC), belong to a specific subgroup within the AAA+ family of proteins[2,3]. Although the stoichiometries and stabilities of initiator assemblies vary among the different domains of life, all require ATP to form an activated complex competent to trigger DNA replication[4,5].

The bacterial protein DnaA has long served as a model for understanding initiator action[6]. The processing of bacterial replication origins requires cooperative, ATP-dependent assembly of DnaA monomers bound to a series of defined 9-base-pair (bp) sequences known as DnaA-boxes[6]. In the presence of DNA-bending architectural factors such as HU and IHF, and using DNA that is destabilized by negative supercoiling, formation of the DnaA nucleoprotein complex triggers the melting of an (A+T)-rich DNA unwinding element (DUE)[7]. After DNA opening, DnaA recruits the DnaB replicative helicase to the origin[8], an event chaperoned by the DnaC helicase-loader protein[9,10]. DnaB loading then facilitates the stepwise assembly of the replisome, beginning with the DnaG primase[10]. In *Escherichia coli*, formation of the first primer-template junction promotes the disassembly of the DnaA nucleoprotein complex through the recruitment of the Hda protein by the DNA polymerase III β subunit processivity clamp. Hda and the β clamp combine to form the regulatory inactivation of DnaA (RIDA) complex, which stimulates the ATPase activity of DnaA to prevent replication reinitiation[11].

DnaA is highly conserved in all bacteria and is readily identifiable by a DnaA signature sequence in its C-terminal DNA-binding domain (domain IV)[6]. This sequence mediates the interaction of DnaA with the equally well-conserved DnaA box sequence[12]. Although the DnaA–DnaA box interaction is highly conserved in all bacteria, the overall number and arrangement of DnaA boxes within replication origins varies greatly, even among related bacterial families[13]. How a conserved initiator protein accommodates this origin heterogeneity has been a puzzling feature of bacterial replication[4,14].

The central AAA+ domain of DnaA is crucial for the cooperative self-assembly that defines nucleoprotein complex formation on origins[6]. To date, structural studies of functional AAA+ assemblies have revealed primarily hexameric, closed-ring particles[3]. The exceptions are the bacterial and eukaryotic clamp loaders[15,16], which form open, split-ring pentamers. In all AAA+ assemblies, ATP binding occurs at the interface between neighboring subunits; one protomer provides the primary nucleotide-binding pocket, defined by the Walker A, Walker B, sensor I and sensor II sequence motifs, whereas the other contributes a conserved arginine residue, characteristic of the box VII (or SRC) motif, to form a bipartite ATP-binding site. With the exception of the sensor II element, a feature that resides in a helical subdomain known as the AAA+ 'lid,' all of these conserved motifs map to the core AAA+ αβα nucleotide-binding fold. Although structural studies of monomeric, ADP-bound DnaA have confirmed the presence of these hallmark AAA+ elements in the bacterial initiator[17], the mechanism by which ATP activates DnaA oligomerization to drive replication-origin remodeling has remained poorly understood. To address these questions, we have determined the structure of ATP-bound DnaA from the thermophilic bacterium *Aquifex aeolicus*.

Division of Biochemistry and Molecular Biology, Molecular and Cell Biology Department, 327B Hildebrand Hall #3206, University of California, Berkeley, California 94720. Correspondence should be addressed to J.M.B. (jmberger@berkeley.edu).

Received 20 April; accepted 25 May; published online 9 July 2006; doi:10.1038/nsmb1115

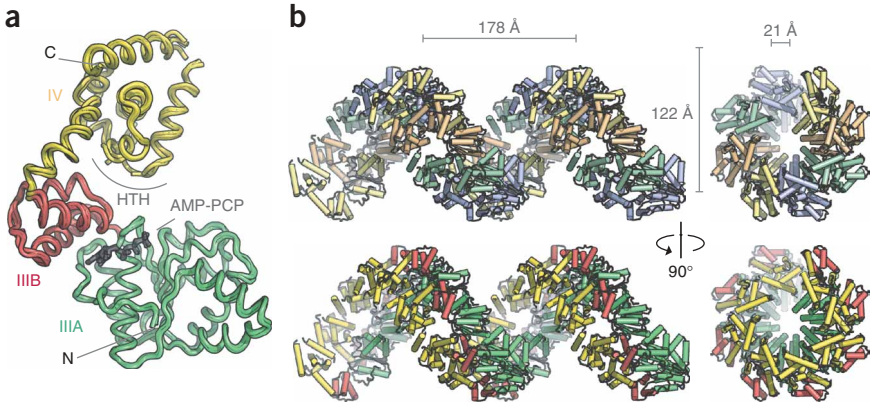

Figure 1 Structure of ATP-DnaA. (**a**) Overlay of the four DnaA monomers in the asymmetric unit. The AAA+ module is colored green and red (domains IIIA and IIIB, respectively); domain IV, the DNA-binding element, is yellow. The ATP analog AMP-PCP is shown as black sticks. The helix-turn-helix (HTH) motif in domain IV and the N and C termini are labeled. (**b**) ATP-DnaA forms a right-handed helical filament with 8_1 symmetry. Side and axial views of four symmetry-related DnaA tetramers are shown. Top, the four monomers in the asymmetric unit are colored blue, green, orange and yellow. Bottom, identical view, but protomers are colored by domain as in **a**.

RESULTS

ATP-DnaA forms a helical AAA+ array

We developed an *in vitro* protocol to exchange bound nucleotides in *A. aeolicus* DnaA with the nonhydrolyzable ATP analog AMP-PCP (see Methods), promoting the growth of a new crystal form of DnaA that diffracted to 3.5-Å resolution. Phase information was obtained by molecular replacement using the AAA+ domain of ADP-bound DnaA as a search model, and a final model was built and refined to an R_{free} of 29.1% with excellent stereochemistry (**Supplementary Fig. 1** online). Each asymmetric unit contains four structurally similar DnaA molecules (**Fig. 1a**) arranged in a head-to-tail manner. When combined with symmetry-related tetramers along a crystallographic two-fold screw axis, ATP-DnaA forms a 122-Å-wide right-handed helical filament that extends along the entire *b*-axis of the crystal (**Fig. 1b** and **Supplementary Video 1** online).

Functional ATP interactions in the ATP-DnaA filament

The AAA+ domain of DnaA is the primary oligomerization determinant of the filament, with adjacent AAA+ modules packing in a manner analogous to other oligomeric AAA+ proteins (**Fig. 2a**). The interaction surface is composed of conserved residues (**Fig. 2b**) in two clusters, one on either side of the nucleotide-binding pocket. The first group is located on the sensor II helix (α11) of one AAA+ module and on two helices (α1 and α8) of the adjacent monomer (**Fig. 2c**). Two conserved glycine residues characterize this interface, allowing for a close packing interaction between helices α11 and α8. Helix α3 is the crucial component of the second contact point, interacting with helices α6 and α4 from the neighboring protomer (**Fig. 2d**).

An analysis of the ATP-DnaA nucleotide-binding site reveals that within the filamentous structure, a number of conserved residues intimately engage ATP (**Fig. 3a**). To validate the functional relevance

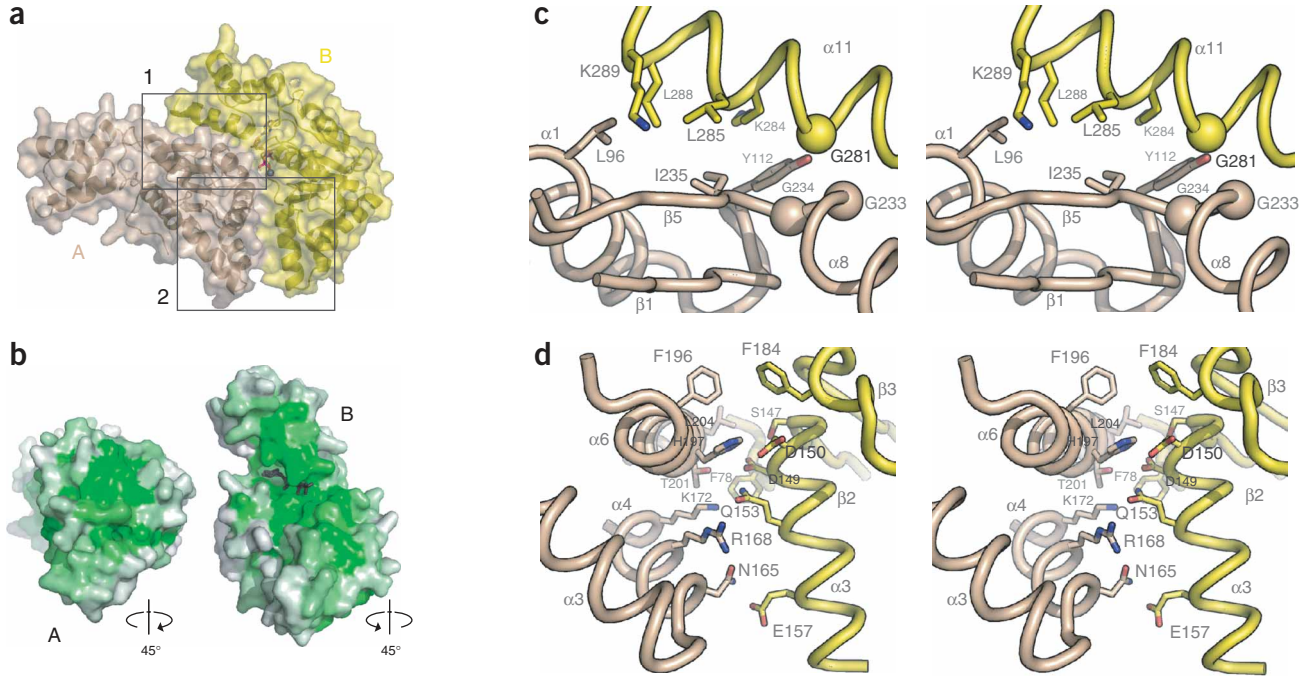

Figure 2 Organization of AAA+ modules in the helical filament. (**a**) The predominant dimer interface occurs between the AAA+ modules of adjacent monomers and centers on two clusters of residues (boxed) on either side of the nucleotide-binding pocket. (**b**) Mapping of a CONSURF conservation analysis (>200 nonredundant sequences) onto the 'exploded' AAA+ interaction surface (green, highly conserved; white, nonconserved). (**c**,**d**) Stereo views of interaction regions 1 (**c**) and 2 (**d**).

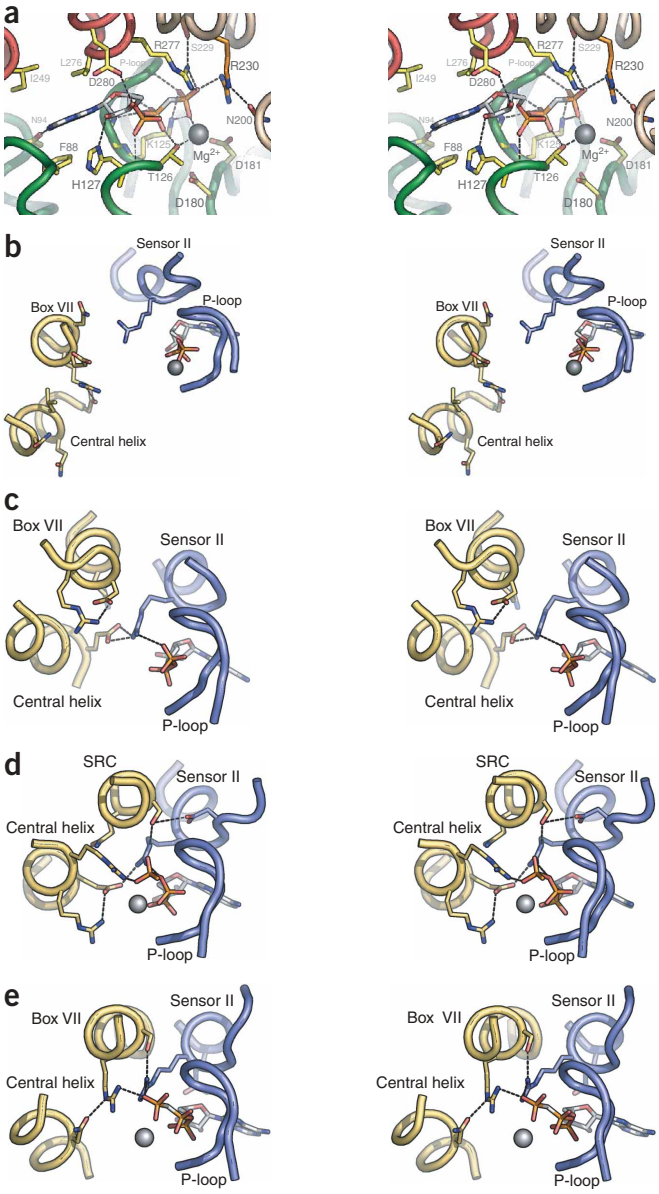

Figure 3 A functional, closed nucleotide-interaction pocket in ATP-DnaA. (**a**) Stereo view of the nucleotide-binding pocket of DnaA showing interactions between the protein and the nucleotide. Domains IIIA and IIIB from monomer B are colored green and red, respectively, and the box VII helix from monomer A is colored salmon. Interactions within hydrogen-bonding distance are shown as dashed lines. (**b**,**c**) Nucleotide-binding pockets of ClpA (**b**; PDB entry 1KSF) and NtrC (**c**; 1NY5) do not intimately contact the nucleotide. The ClpA interface is completely open, whereas the NtrC arrangement positions the predicted arginine finger away from the nucleotide and does not contain a Mg^{2+} ion. (**d**,**e**) Nucleotide-binding pockets of RFC-AB (**d**; 1SXJ) and ATP-DnaA (**e**) are closed and characterized by intimate contacts derived from both AAA+ subunits.

of the active site formed within the DnaA filament, we compared the ATP-binding pocket of DnaA to those of other AAA+ assemblies. Several structurally characterized AAA+ proteins adopt quaternary structures in crystal packing lattices that are believed to represent noncatalytic assemblies. These include the NtrC transcription regulator, which crystallized as a closed-ring heptamer, and ClpA, a tandem AAA+ protease that crystallized as a monomer, but with a filament-like assembly along a crystallographic $P6_5$ symmetry axis[18,19]. The bipartite ATP-interaction pocket is notably disrupted in these assemblies, leading to an active site arrangement that either is 'open' (**Fig. 3b**) or does not appropriately position conserved catalytic residues from the SRC motif with bound nucleotide at the oligomerization interface (**Fig. 3c**). By contrast, assemblies thought to approximate catalytic intermediates, such as the RFC eukaryotic clamp-loader complex, have a 'closed' active site geometry and appropriately bind nucleotide using conserved residues from neighboring AAA+ protomers (**Fig. 3d**). The configuration adopted by ATP-DnaA is that of a closed assembly, with a highly organized nucleotide-binding pocket (**Fig. 3e**). The precise geometry of these contacts is dependent on the subunit arrangement arising from the ATP-DnaA spiral, strongly supporting the physiological relevance of the helical filament architecture.

A steric wedge establishes the DnaA superhelix

Within the ATP-DnaA assembly, subunit interfaces are shifted and rotated upward to impose a 14.2-Å lateral displacement that gives rise to the helical superstructure. The extent of this shift is unique among AAA+ proteins; RFC, the only functional AAA+ assembly with a nonplanar quaternary structure, has a maximal out-of-plane displacement of 5.5 Å[15]. Accordingly, the central axis of the DnaA helix is offset from those of planar, ring-shaped AAA+ assemblies such as the D2 domain of NSF[20,21] by $\geq 40^{\circ}$ (**Fig. 4a**).

A recent classification of AAA+ proteins has revealed that bacterial, archaeal and eukaryotic initiators all share a specific helical insert in their ATPase cores[2]. In DnaA, this 'initiator' helix (α3), along with α4, forms a V-shaped 'steric wedge' that protrudes away from the core AAA+ fold, when compared to classic AAA+ proteins such as NSF (**Fig. 4b**,**c**). In the context of the filament, these wedges guide adjacent subunits into a nonplanar arrangement by reorienting the AAA+ interface, directly preventing the flat ring assembly observed in NSF (**Fig. 4d**).

ATP toggles a conformational switch to promote assembly

A key question in the function of DnaA revolves around the way that ATP promotes self-assembly at replication origins. Our structure, along with the previously solved ADP-bound structure of DnaA, reveals the molecular mechanism for this process. Whereas the α3-α4 wedge directs the helical architecture of DnaA, an ATP-specific conformational change within the AAA+ domain accommodates and stabilizes subunit-subunit interactions necessary to support oligomer formation. This rearrangement is crucial for filament formation, as the relative positions of domains IIIA and IIIB in the ADP structure are not sterically compatible with the helical assembly (**Fig. 5a**,**b**). Indeed, it is the presence of the γ-phosphate of AMP-PCP that enables a number of conserved protein-nucleotide interactions to be formed. The repositioning of the lid domain is anchored by a contact between the γ-phosphate and the invariant sensor II arginine (Arg277(Arg334); corresponding *E. coli* residues are identified in parentheses), and one between another conserved lid residue, Glu280(Glu337), and the 2′-OH of the bound nucleotide (**Fig. 5c**). The rearrangement of the domain IIIB lid opens the face of the AAA+ module to allow the box VII helix from a neighboring protomer to occupy the space vacated by the displaced sensor II helix (**Fig. 5b**,**c** and **Supplementary Video 2** online). Within the oligomeric assembly, the box VII helix engages the nucleotide with a single conserved residue, Arg230(Arg285). This residue, which is essential for DnaA function[22,23], acts as an 'arginine finger,' coupling ATP binding and DnaA self-assembly. The position of

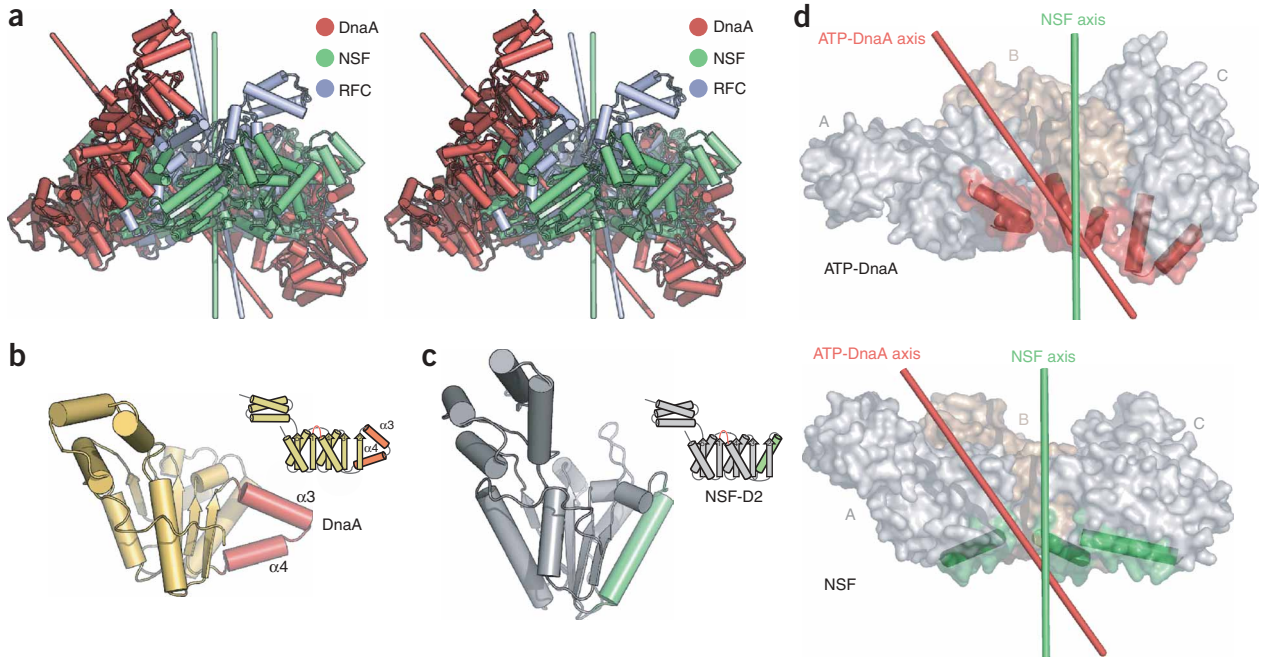

Figure 4 The initiator helical insert drives filament formation. (**a**) The ATP-DnaA helix defines a novel AAA+ assembly mode. Stereo view of NSF (PDB entry 1D2N), RFC (1SXJ) and DnaA assemblies (AAA+ domains only) superposed by least-squares fitting of the nucleotide-binding core of a single AAA+ monomer from each assembly. The central symmetry axes of each assembly are depicted as rods. (**b**,**c**) Ribbon and topology diagrams of DnaA (**b**) and NSF (**c**; 1D2N), showing the initiator-specific helical insert in red and the classic AAA+ helix 2 in green. (**d**) Helices α3 and α4 of DnaA (top) form a V-shaped steric wedge that blocks assembly of DnaA domains into a closed, planar array like NSF (bottom).

Arg230(Arg285) is guided by a hydrogen bond to a conserved asparagine, Asn200(Asn232), on α6. The box VII helix further promotes the stability of the assembly by engaging the sensor II arginine with a polar residue, Ser229(Ser284). This serine, which immediately precedes the arginine finger, is a highly conserved feature of the box VII/SRC region in a large subset of AAA+ proteins. Its similar positioning in ATP-DnaA and in the A and B subunits of RFC suggests that it functions to orient the sensor II arginine in active assemblies of these enzymes.

Mutagenesis studies in *E. coli* have examined the roles of a number of these nucleotide interactions *in vitro* and *in vivo*. Mutating the sensor II arginine to histidine, although it reduces the hydrolysis rate of DnaA, does not prevent oligomerization of ATP-DnaA[24]. This result indicates that the conformational change necessary for assembly is not strictly dependent on the interaction of Arg277(Arg334) with the γ-phosphate. In contrast, mutating the box VII arginine, Arg230(Arg285), to alanine prevents the formation of an active nucleoprotein complex[23], suggesting that engagement of ATP by this residue may be a dominant factor stabilizing the conformational switch. In addition to Arg230(Arg285), bacterial box VII sequences contain a second invariant arginine, Arg226(Arg281). In our structure, there is only weak density for the side chain of this residue and no evidence that it interacts with the γ-phosphate. Mutant DnaA proteins containing an alanine substitution at this position can bind ATP and form a nucleoprotein complex that is competent for origin unwinding, but cannot recruit the DnaB–DnaC helicase-loading complex[22]. The molecular interactions observed in our structure are thus consistent with the mutagenesis data and explain the distinct functional roles for Arg226(Arg281), Arg230(Arg285) and Arg277(Arg334) in filament assembly and ATP hydrolysis.

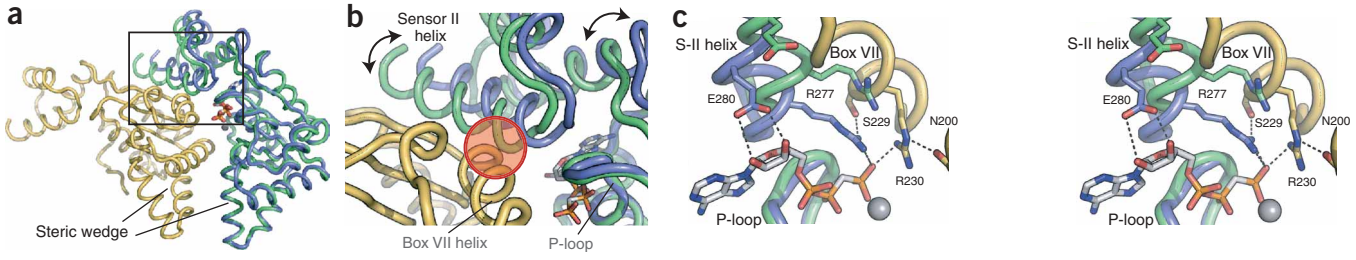

Figure 5 Conformational changes induced by ATP binding. (**a**) ATP-DnaA dimer (blue and gold) with ADP-DnaA (green; PDB entry 1L8Q) superposed on one subunit. (**b**) Detail, with arrows indicating movement of the AAA+ lid (DnaA domain IIIB) required to accommodate a steric clash that occurs in the ADP-DnaA AAA+ orientation (red circle). (**c**) Stereo view of the molecular features of the ADP-to-ATP switch. The lid movement is stabilized by interactions of the sensor II (SII) arginine with the γ-phosphate and enables the box VII helix to engage the nucleotide through the arginine finger (Arg230). Further stability is provided by interactions of Glu280 with the ribose ring and of the box VII residue Ser229 with Arg277.

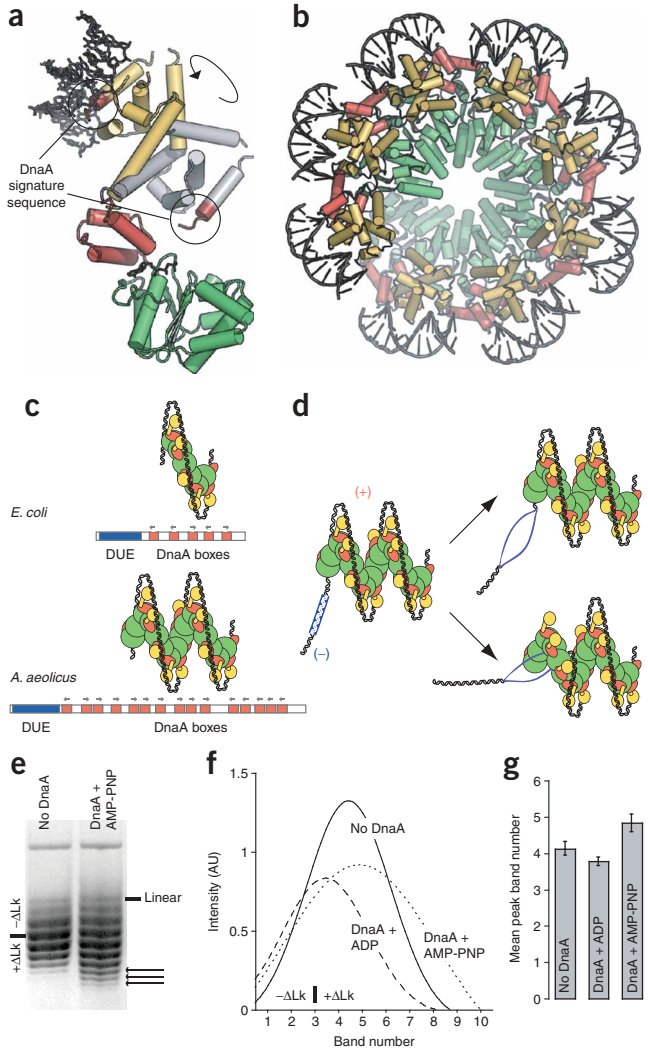

Figure 6 The DnaA filament in the context of the nucleoprotein complex. (**a**) DNA engagement by oligomerized DnaA requires a rotation of the DNA-binding domain (yellow) about the hinge at the base of the connector helix from its position in the filament (gray). DNA is modeled onto domain IV on the basis of the *E. coli* domain IV–DNA cocrystal structure (PDB entry 1J1V). (**b**) The outward rotation orients DNA on the outside of the helical assembly, as predicted from EM and DNA-protection studies[8,25]. (**c**) Modulation of filament size enables the engagement of origins of different lengths with highly diverse numbers of DnaA boxes (shown in red; orientations indicated by arrows), exemplified by the *E. coli* and *Aquifex* origins. (**d**) Filament formation generated by positive supercoiling may destabilize the origin unwinding element through compensatory negative supercoiling strain (top arrow). Coincident with or after opening, the axial channel of ATP-DnaA may directly engage the unwound DUE (bottom arrow). (**e**) Representative DNA topology footprint analyzed on a chloroquine-containing agarose gel shows that ATP-DnaA shifts the topoisomer equilibrium in the positive direction (arrows) compared to reactions with no protein or to ADP-DnaA controls (data not shown). (**f**) Gaussian distribution of band intensities from a comparative set of topology footprint experiments. (**g**) Histogram of the mean peak band numbers for DnaA-free, ADP-DnaA and ATP-DnaA topology footprint experiments. Error bars show s.d. from three independent footprinting runs.

ATP-DnaA stabilizes positive DNA supercoils

The mechanism that enables the DnaA oligomer to render an origin competent for replisome assembly is poorly understood. Domain IV of DnaA is an independent origin-binding domain that specifically targets DnaA monomers to DnaA box repeats[6,12]. In the ADP-DnaA structure, domain IV is linked to the AAA+ domain by an extended, but straight, α-helix[17]. In ATP-DnaA, the relative position of domain IV is constant between the four DnaA molecules in the asymmetric unit (**Fig. 1a**), but the linker helix is substantially bent, reorienting the DNA-binding domain by ~45° in comparison to the ADP-DnaA structure. These differences demonstrate that the ATPase and DNA-binding domains of DnaA are tethered, but conformationally uncoupled. Consistent with this observation, modeling studies using the *E. coli* domain IV–DNA cocrystal structure[12] indicate that domain IV must pivot around the domain III–domain IV linker helix and project radially outward from the AAA+ axis to engage duplex DNA in a manner sterically compatible with the helical filament (**Fig. 6a**,**b**). This arrangement is consistent with previously proposed models based on footprint protection patterns[25] and EM micrographs of the *E. coli* nucleoprotein complex[8], which have predicted that origin DNA wraps around the outside of a DnaA core.

The helical structure of the ATP-DnaA oligomer offers a new framework to consider how the initiator engages and melts replication origins. For example, it is well established that the origins of different bacteria vary greatly in length and number of DnaA boxes. A filamentous DnaA assembly provides a ready mechanism for accommodating this heterogeneity, as it could grow or shrink at either end in a manner dependent on the size and organization of the origin (**Fig. 6c**). Recent studies have also established that higher-order chromosome organization exists in a number of bacterial species[26], generating defined diffusion barriers that divide chromosomes into topological domains[27]. As a right-handed ATP-DnaA spiral would be expected to wrap DNA into a positive supercoil, adjacent DNA regions would be subjected to compensatory negative writhe (**Fig. 6d**, left). Although any superhelical strain generated by DnaA-mediated wrapping would be expected to spread throughout the topological domain that contains the origin, it may preferentially affect the nearby DUE, which is unstable and prone to spontaneous unwinding (**Fig. 6d**, top arrow).

To test whether ATP-bound DnaA indeed stabilizes a positive wrap, we used a 'topology footprint' assay to investigate the activity of ATP-DnaA and ADP-DnaA on plasmid DNA containing the DnaA box repeats found in the *A. aeolicus* replication origin. *Aquifex oriC* contains 15 DnaA boxes, which together span ~350 bp[13] (**Supplementary Fig. 2** online). We chose *Aquifex* as our model system because we can precisely control the nucleotide binding state of its DnaA protein and because the helical structure we observed indicates that any topological changes induced upon oligomerization should be more pronounced owing to the large number of DnaA boxes in the origin.

The addition of ATP-DnaA (trapped with AMP-PNP) led to a marked shift in the distribution of topoisomers toward more positively supercoiled species (**Fig. 6e**), an effect not observed in DnaA-free reactions or with ADP-DnaA (**Fig. 6f**,**g**). This result demonstrates that *Aquifex* DnaA stabilizes a positive-handed DNA wrap in the presence of ATP, a result consistent with the observed right-handed filament (**Fig. 1b**). Notably, a similar effect, also dependent on the presence of nonhydrolyzable ATP analogs, was observed with a control plasmid that lacks the *Aquifex* DnaA box repeats (data not shown). We attribute this behavior to the presence of cryptic DnaA boxes in the control plasmid, as previous studies in *E. coli* have shown that a single DnaA box is sufficient to promote DnaA protection of adjacent DNA regions in a nonspecific manner[28,29]. Although additional factors probably promote the interaction between ATP-DnaA and its cognate DNA–binding sites to improve the

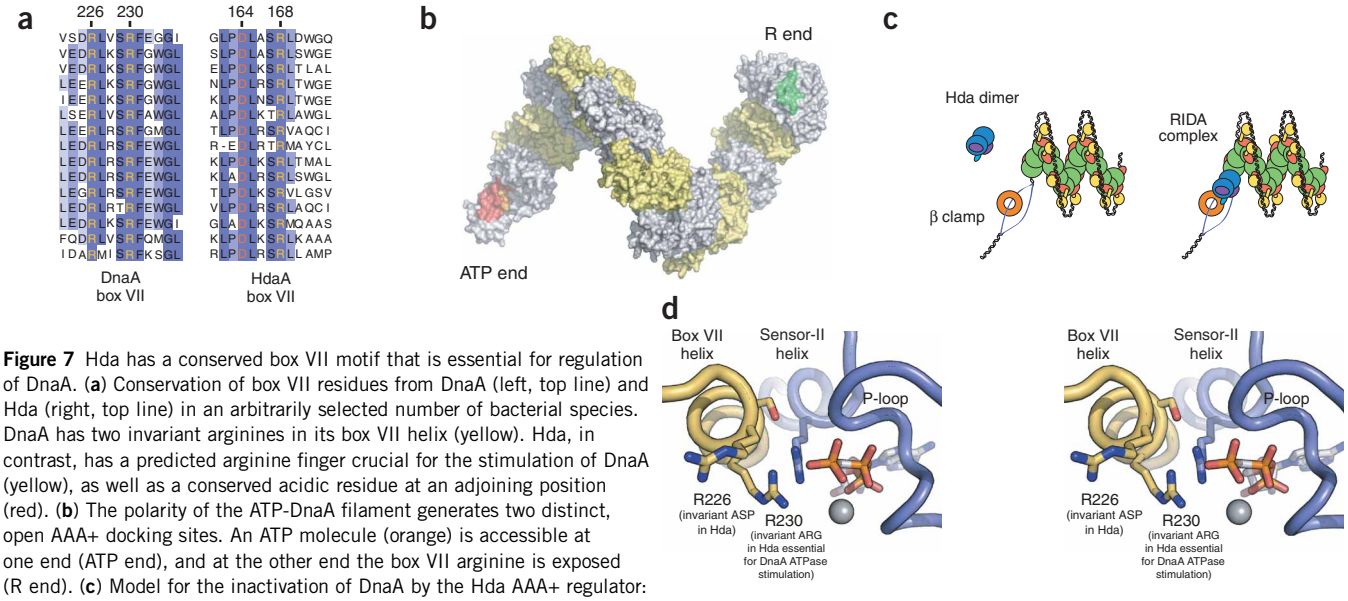

Figure 7 Hda has a conserved box VII motif that is essential for regulation of DnaA. (**a**) Conservation of box VII residues from DnaA (left, top line) and Hda (right, top line) in an arbitrarily selected number of bacterial species. DnaA has two invariant arginines in its box VII helix (yellow). Hda, in contrast, has a predicted arginine finger crucial for the stimulation of DnaA (yellow), as well as a conserved acidic residue at an adjoining position (red). (**b**) The polarity of the ATP-DnaA filament generates two distinct, open AAA+ docking sites. An ATP molecule (orange) is accessible at one end (ATP end), and at the other end the box VII arginine is exposed (R end). (**c**) Model for the inactivation of DnaA by the Hda AAA+ regulator: β clamp (orange) deposition at the origin promotes the recruitment of an Hda dimer (blue) to form the RIDA complex. RIDA interacts with the exposed ATP end of the DnaA filament, promoting ATP hydrolysis and inactivating DnaA. (**d**) Stereo view of the ATP-DnaA nucleotide-binding pocket, showing the predicted positions of conserved Hda box VII residues crucial for the formation of a heterodimeric ATP-binding pocket.

specificity of origin recognition and couple initiator self-assembly with DUE opening *in vivo*[7], the topology footprints presented here are consistent with a model for DNA engagement in which DnaA stabilizes a right-handed DNA wrap in an ATP-dependent manner.

DISCUSSION

Evidence for a secondary DNA-interaction surface

In addition to providing a mechanism for self-assembly, the ATP-DnaA structure also helps explain a number of biochemical and biological properties of the bacterial initiator. For example, DNA footprinting studies have shown that ATP-DnaA, but not ADP-DnaA, engages degenerate DnaA box sequences (I-sites) in *oriC*[30] as well as 'ATP-DnaA box' sequences in the (A+T)-rich DUE[29,31]. Whereas I-site binding probably arises from additional, cooperative interactions of origin DNA with domain IV, protection of the unwinding element suggests DnaA has additional DNA-binding modes. Phylogenetic analysis of the DnaA AAA+ domain reveals a number of conserved amino acid residues in the axial channel and upper surface of the helical assembly (**Supplementary Fig. 3** online). These regions also form the most electropositive surfaces of the AAA+ portion of the DnaA oligomer. Given the examples of AAA+ helicases and the clamp-loader complex[15,32], this pattern suggests that the central channel of the ATP-DnaA filament may comprise a secondary DNA-binding region. A small redirection of the DNA wrap from the outside of the helix to the inside (**Fig. 6d**, bottom arrow), perhaps facilitated by architectural factors, could allow the AAA+ domains of DnaA to act directly on DUEs, perhaps in a manner analogous to AAA+ translocases. In this regard, it is noteworthy that formation of a helical open ring, unlike a closed toroid, would permit unfettered access to this conserved, electrostatically positive surface. Such an interaction would be consistent with the extended DUE footprints specifically observed for ATP-bound DnaA[29].

AAA+ protein interactions during replication initiation

During initiation, *E. coli* DnaA interacts with several replication proteins, including the regulatory factor Hda[11] and the DnaB–DnaC helicase-loader assembly[8,33]. Hda is an essential component of the RIDA complex in *E. coli*[11] and a DnaA paralog. RIDA prevents overinitiation by shifting active ATP-DnaA into an inactive, ADP-bound state[34]. The recent *in vitro* reconstitution of RIDA activity has revealed that a conserved arginine residue in the Hda box VII helix (**Fig. 7a**) is essential for stimulating the ATPase activity of DnaA[35], indicating that the contact between Hda and DnaA is a canonical AAA+ interaction. Although this type of association is difficult to reconcile with a closed-ring AAA+ assembly, where there are no exposed AAA+ interfaces, it can be explained readily if the exposed ends of an ATP-DnaA filament serve as docking sites (**Fig. 7b,c**). On the basis of this observation and our structure, Hda can be predicted to bind the open, 'front' face of the ATP-DnaA superhelix, generating a heterodimeric ATP-binding pocket that is competent for hydrolysis (**Fig. 7d**). Notably, instead of the second conserved box VII arginine, Hda has an invariant aspartate at this position (**Fig. 7a,d**), a change that may be coupled to the ability of Hda to increase the rate of ATP hydrolysis by DnaA. Because the γ-phosphate is important for stabilizing the ATP-DnaA oligomer, Hda-promoted hydrolysis at one end, if propagated throughout the filament, would facilitate nucleoprotein-complex disassembly and prevent reinitiation.

Another important function for DnaA during initiation is to coordinate proper recruitment and deposition of the DnaB helicase onto a newly unwound replication origin. Although this event is dependent upon an association between the N-terminal domain of DnaA and DnaB[36,37], the presence of the DnaC helicase-loader protein is also required. DnaC, like Hda, is an AAA+ DnaA paralog. This relationship raises the possibility that DnaC directly engages the exposed AAA+ surfaces at the open ends of an ATP-DnaA superhelix, an association that would serve to further regulate helicase recruitment and loading.

Conserved cellular initiator architecture

The structural similarities between the AAA+ domains of archaeal and bacterial initiators have led to suggestions that these proteins share

substantial mechanistic properties[17,38]. The observation that an α-helical steric wedge (**Fig. 4b**) is a common feature of all initiators[2] raises the question of whether the AAA+ domains of archaeal and eukaryotic initiators assemble and pack together in a manner similar to that seen in ATP-DnaA. In contrast to initiation in *E. coli*, where DNA unwinding and helicase recruitment have been biochemically reconstituted *in vitro*, our understanding of archaeal and eukaryotic initiation is more limited. Nonetheless, there is evidence that these initiators, like DnaA, also can alter DNA superstructure[39]. Moreover, the nucleotide-dependent interaction between Cdc6 and ORC during eukaryotic initiation[40,41], as well as the recent observation that nucleotide binding is crucial for stable assembly of human ORC[42], are congruent with our model for DnaA assembly and regulation, and they suggest that an open-ended, spiral AAA+ substructure is a universal architectural feature of all cellular initiators. Consistent with this proposal, EM reconstructions of *Drosophila melanogaster* ORC reveal a helical feature within the complex that accommodates a five-subunit, DnaA-like AAA+ assembly, but not other types of higher-order AAA+ architectures[43]. This finding indicates that the DnaA oligomer is a useful model to further our understanding of higher-order initiator architecture and function in all domains of life.

METHODS

Protein purification and crystallization. MBP-fused *A. aeolicus* DnaA (residues 77–399) was purified as described previously[17], except for a few modifications, as follows. To remove residual ADP that was stably bound by the protein, 2 mM EDTA was added to peak heparin column fractions before fractionation over a Sephacryl S-300 gel-filtration column in chelating buffer (50 mM HEPES (pH 7.5), 500 mM KCl, 10% (v/v) glycerol, 2 mM EDTA). Peak fractions were pooled and incubated with 15 mM $MgCl_2$ and 0.1 mM β,γ-methyleneadenosine 5′-triphosphate (AMP-PCP) for 1 h at room temperature, then cleaved with His-tagged tobacco etch virus protease for 20 h at 18 °C. After repassage over a 2-ml His-Trap column to remove uncleaved product, DnaA was heat-treated for 15 min at 65 °C, centrifuged for 20 min at 4 °C and gel-filtered over an S-200 column in crystallization buffer (25 mM HEPES (pH 7.5), 250 mM KBr, 250 mM KCl, 10% (v/v) glycerol, 10 mM $MgCl_2$, 20 μM AMP-PCP). Peak fractions were then pooled and concentrated to 20 mg ml^{-1}.

ATP-DnaA crystals were grown using hanging drop vapor diffusion by mixing 1 μl protein and 1 μl well solution (25 mM sodium cacodylate (pH 6.5), 24%–26% (v/v) 1,2-propanediol and 10% (w/v) PEG MME 2,000). Rod-like crystals (approximately 300 μm × 30 μm × 30 μm) grew in 1–2 d and reached maximal size after 3–5 d. Crystals were harvested directly from drops and flash-frozen in liquid nitrogen before data collection.

Structure determination. Data were collected from a single crystal at beamline 8.3.1 at the Advanced Light Source at a wavelength of 1.1159 Å and processed using DENZO/SCALEPACK[44]. The crystals belong to space group $P2_12_12_1$, with unit cell dimensions $a = 99.1$ Å, $b = 117.7$ Å and $c = 201.0$ Å and a solvent content of approximately 68% (**Table 1**). To prevent loss of signal from radiation damage, partial data sets were collected by translating a 30-μm X-ray beam along the length of the crystals and then merged. The limited completeness of the 3.5-Å data set (**Table 1**) is a direct consequence of radiation damage, small crystal size and an inability to merge data from different crystals owing to extreme nonisomorphism along the *b*-axis of the crystals. A polyalanine model of residues 77–290 of ADP-DnaA calculated using PHASER[45] gave a single molecular-replacement solution. After rigid-body fitting of domains IIIa and IIIb using CNS[46], the DNA-binding domain was manually docked into visible density. RESOLVE prime and switch[47] and CNS composite anneal omit maps[46] were used for manual rebuilding in O[48]. Positional refinement was performed with REFMAC[49] and grouped *B* refinement with CNS[46]. The final model contains all residues except the following positions: 329–330, 359–360 and 379–380 in chain A; 328, 360–361 and 379–380 in chain B; 328, 359–361 and 379–380 in chain C; and 328 and 379–380 in chain D. In the final model, 81.1%, 18.2% and 0.8% of residues fall within favored, additionally allowed and generously allowed regions of Ramachandran space, respectively. Surface conservation and electrostatic potentials were determined using CONSURF[50] and GRASP[51]. Figures were generated using PyMOL (http://pymol.sourceforge.net).

Table 1 Data collection and refinement statistics

	AMP-PCP crystal
Data collection	
Space group	$P2_12_12_1$
Cell dimensions	
a, *b*, *c* (Å)	99.08, 117.71, 200.99
Resolution (Å)	50–3.5 (3.63–3.5)[a]
R_{sym} (%)	13.7 (45.5)
$I / \sigma I$	6.6 (1.9)
Completeness (%)	86.3 (84.8)
Redundancy	3.6 (3.1)
Refinement	
Resolution (Å)	30 (3.5)
No. reflections	24,077 (1,293)[b]
R_{work} / R_{free} (%)	26.4 / 29.1
No. atoms	
Protein	10,437
Ligand/ion	128
B-factors	
Protein	99.1
Ligand/ion	40.0
R.m.s deviations	
Bond lengths (Å)	0.008
Bond angles (°)	1.07

[a]Highest-resolution shell shown in parentheses. [b]Number of test reflections shown in parentheses.

Topology footprint assay. The region of the predicted *A. aeolicus* replication origin containing DnaA-box repeats[13] (nucleotides 166927–167250 of GenBank entry NC-000918) was PCR-amplified and cloned into a modified pET vector (LICpET3aTr). Topology footprint reactions were carried out in 100 μl of reaction buffer (75 mM NaCl, 50 mM Tris (pH 7.9), 10 mM DTT, 5 mM $MgCl_2$, 100 mg ml^{-1} BSA, 10% (v/v) glycerol) containing 1.5 μg of DNA (4.3 nM) and 2 μg poly(dI/dC). MBP-fused, nucleotide-free *Aquifex* DnaA was incubated with 2 mM β,γ-imidoadenosine 5′-triphosphate (AMP-PNP) or ADP for 15 min and added at various concentrations (0.45–2.7 μM) to the reaction mixture. After a 15-min incubation at 25 °C, 2.5 units of wheat germ topoisomerase I was added, and the mixture was incubated 45 min at 25 °C. 100 μl of 1% (w/v) SDS and 10 mM EDTA was used to stop the reactions and the DNA was purified by phenol-chloroform extraction and ethanol precipitation. Samples were loaded on a 1% agarose gel containing 1.4 μg ml^{-1} chloroquine, run at 23 V for 30–36 h and visualized by ethidium bromide staining. A maximum shift was observed at a DnaA concentration of 1.8 μM, which represents a 30-fold molar excess of DnaA over DnaA boxes. Topoisomer distributions from multiple independent runs were quantitated by ImageQuant software.

Accession codes. Protein Data Bank: Coordinates have been deposited with accession code 2HCB.

Note: Supplementary information is available on the Nature Structural & Molecular Biology website.

ACKNOWLEDGMENTS

We thank J. Holton and J. Tanamachi for support at Advanced Light Source beamline 8.3.1 and A. Schoeffler for purifying Topo IB. N. Cozzarelli, M. Botchan, J. Kuriyan, J. Keck, J. Stray and members of the Berger laboratory provided helpful comments and suggestions. This work was supported by the G. Harold and Leila Y. Mathers Charitable Foundation and the US National Institutes of Health (GM071747).

COMPETING INTERESTS STATEMENT
The authors declare that they have no competing financial interests.

Published online at http://www.nature.com/nsmb/
Reprints and permissions information is available online at http://npg.nature.com/reprintsandpermissions/

1. Giraldo, R. Common domains in the initiators of DNA replication in Bacteria, Archaea and Eukarya: combined structural, functional and phylogenetic perspectives. *FEMS Microbiol. Rev.* **26**, 533–554 (2003).
2. Iyer, L.M., Leipe, D.D., Koonin, E.V. & Aravind, L. Evolutionary history and higher order classification of AAA+ ATPases. *J. Struct. Biol.* **146**, 11–31 (2004).
3. Erzberger, J.P. & Berger, J.M. Evolutionary relationships and structural mechanisms of AAA+ proteins. *Annu. Rev. Biophys. Biomol. Struct.* **35**, 93–114 (2006).
4. Robinson, N.P. & Bell, S.D. Origins of DNA replication in the three domains of life. *FEBS J.* **272**, 3757–3766 (2005).
5. Lee, D.G. & Bell, S.P. ATPase switches controlling DNA replication initiation. *Curr. Opin. Cell Biol.* **12**, 280–285 (2000).
6. Messer, W. The bacterial replication initiator DnaA. DnaA and oriC, the bacterial mode to initiate DNA replication. *FEMS Microbiol. Rev.* **26**, 355–374 (2002).
7. Leonard, A.C. & Grimwade, J.E. Building a bacterial orisome: emergence of new regulatory features for replication origin unwinding. *Mol. Microbiol.* **55**, 978–985 (2005).
8. Funnell, B.E., Baker, T.A. & Kornberg, A. In vitro assembly of a prepriming complex at the origin of the *Escherichia coli* chromosome. *J. Biol. Chem.* **262**, 10327–10334 (1987).
9. Davey, M.J., Fang, L., McInerney, P., Georgescu, R.E. & O'Donnell, M. The DnaC helicase loader is a dual ATP/ADP switch protein. *EMBO J.* **21**, 3148–3159 (2002).
10. Fang, L., Davey, M.J. & O'Donnell, M. Replisome assembly at oriC, the replication origin of *E. coli*, reveals an explanation for initiation sites outside an origin. *Mol. Cell* **4**, 541–553 (1999).
11. Kato, J. & Katayama, T. Hda, a novel DnaA-related protein, regulates the replication cycle in *Escherichia coli*. *EMBO J.* **20**, 4253–4262 (2001).
12. Fujikawa, N. *et al.* Structural basis of replication origin recognition by the DnaA protein. *Nucleic Acids Res.* **31**, 2077–2086 (2003).
13. Mackiewicz, P., Zakrzewska-Czerwinska, J., Zawilak, A., Dudek, M.R. & Cebrat, S. Where does bacterial replication start? Rules for predicting the oriC region. *Nucleic Acids Res.* **32**, 3781–3791 (2004).
14. Cunningham, E.L. & Berger, J.M. Unraveling the early steps of prokaryotic replication. *Curr. Opin. Struct. Biol.* **15**, 68–76 (2005).
15. Bowman, G.D., O'Donnell, M. & Kuriyan, J. Structural analysis of a eukaryotic sliding DNA clamp-clamp loader complex. *Nature* **429**, 724–730 (2004).
16. Jeruzalmi, D., O'Donnell, M. & Kuriyan, J. Crystal structure of the processivity clamp loader gamma (gamma) complex of *E. coli* DNA polymerase III. *Cell* **106**, 429–441 (2001).
17. Erzberger, J.P., Pirruccello, M.M. & Berger, J.M. The structure of bacterial DnaA: implications for general mechanisms underlying DNA replication initiation. *EMBO J.* **21**, 4763–4773 (2002).
18. Lee, S.Y. *et al.* Regulation of the transcriptional activator NtrC1: structural studies of the regulatory and AAA+ ATPase domains. *Genes Dev.* **17**, 2552–2563 (2003).
19. Guo, F., Maurizi, M.R., Esser, L. & Xia, D. Crystal structure of ClpA, an Hsp100 chaperone and regulator of ClpAP protease. *J. Biol. Chem.* **277**, 46743–46752 (2002).
20. Lenzen, C.U., Steinmann, D., Whiteheart, S.W. & Weis, W.I. Crystal structure of the hexamerization domain of N-ethylmaleimide-sensitive fusion protein. *Cell* **94**, 525–536 (1998).
21. Yu, R.C., Hanson, P.I., Jahn, R. & Brunger, A.T. Structure of the ATP-dependent oligomerization domain of N-ethylmaleimide sensitive factor complexed with ATP. *Nat. Struct. Biol.* **5**, 803–811 (1998).
22. Felczak, M.M. & Kaguni, J.M. The box VII motif of *Escherichia coli* DnaA protein is required for DnaA oligomerization at the E. coli replication origin. *J. Biol. Chem.* **279**, 51156–51162 (2004).
23. Kawakami, H., Keyamura, K. & Katayama, T. Formation of an ATP-DnaA-specific initiation complex requires DnaA Arginine 285, a conserved motif in the AAA+ protein family. *J. Biol. Chem.* **280**, 27420–27430 (2005).
24. Su'etsugu, M. *et al.* DNA replication-coupled inactivation of DnaA protein in vitro: a role for DnaA arginine-334 of the AAA+ Box VIII motif in ATP hydrolysis. *Mol. Microbiol.* **40**, 376–386 (2001).
25. Bramhill, D. & Kornberg, A. A model for initiation at origins of DNA replication. *Cell* **54**, 915–918 (1988).
26. Thanbichler, M., Viollier, P.H. & Shapiro, L. The structure and function of the bacterial chromosome. *Curr. Opin. Genet. Dev.* **15**, 153–162 (2005).
27. Postow, L., Hardy, C.D., Arsuaga, J. & Cozzarelli, N.R. Topological domain structure of the *Escherichia coli* chromosome. *Genes Dev.* **18**, 1766–1779 (2004).
28. Fuller, R.S., Funnell, B.E. & Kornberg, A. The dnaA protein complex with the *E. coli* chromosomal replication origin (oriC) and other DNA sites. *Cell* **38**, 889–900 (1984).
29. Speck, C. & Messer, W. Mechanism of origin unwinding: sequential binding of DnaA to double- and single-stranded DNA. *EMBO J.* **20**, 1469–1476 (2001).
30. McGarry, K.C., Ryan, V.T., Grimwade, J.E. & Leonard, A.C. Two discriminatory binding sites in the *Escherichia coli* replication origin are required for DNA strand opening by initiator DnaA-ATP. *Proc. Natl. Acad. Sci. USA* **101**, 2811–2816 (2004).
31. Yung, B.Y. & Kornberg, A. The dnaA initiator protein binds separate domains in the replication origin of *Escherichia coli*. *J. Biol. Chem.* **264**, 6146–6150 (1989).
32. Gai, D., Zhao, R., Li, D., Finkielstein, C.V. & Chen, X.S. Mechanisms of conformational change for a replicative hexameric helicase of SV40 large tumor antigen. *Cell* **119**, 47–60 (2004).
33. Marszalek, J. & Kaguni, J.M. DnaA protein directs the binding of DnaB protein in initiation of DNA replication in *Escherichia coli*. *J. Biol. Chem.* **269**, 4883–4890 (1994).
34. Su'etsugu, M., Takata, M., Kubota, T., Matsuda, Y. & Katayama, T. Molecular mechanism of DNA replication-coupled inactivation of the initiator protein in *Escherichia coli*: interaction of DnaA with the sliding clamp-loaded DNA and the sliding clamp-Hda complex. *Genes Cells* **9**, 509–522 (2004).
35. Su'etsugu, M., Shimuta, T.R., Ishida, T., Kawakami, H. & Katayama, T. Protein associations in DnaA-ATP hydrolysis mediated by the Hda-replicase clamp complex. *J. Biol. Chem.* **280**, 6528–6536 (2005).
36. Marszalek, J. *et al.* Domains of DnaA protein involved in interaction with DnaB protein, and in unwinding the *Escherichia coli* chromosomal origin. *J. Biol. Chem.* **271**, 18535–18542 (1996).
37. Sutton, M.D., Carr, K.M., Vicente, M. & Kaguni, J.M. Escherichia coli DnaA protein. The N-terminal domain and loading of DnaB helicase at the *E. coli* chromosomal origin. *J. Biol. Chem.* **273**, 34255–34262 (1998).
38. Kelman, L.M. & Kelman, Z. Archaea: an archetype for replication initiation studies? *Mol. Microbiol.* **48**, 605–615 (2003).
39. Remus, D., Beall, E.L. & Botchan, M.R. DNA topology, not DNA sequence, is a critical determinant for *Drosophila* ORC-DNA binding. *EMBO J.* **23**, 897–907 (2004).
40. Takahashi, N., Tsutsumi, S., Tsuchiya, T., Stillman, B. & Mizushima, T. Functions of sensor 1 and sensor 2 regions of *Saccharomyces cerevisiae* Cdc6p *in vivo* and *in vitro*. *J. Biol. Chem.* **277**, 16033–16040 (2002).
41. Randell, J.C., Bowers, J.L., Rodriguez, H.K. & Bell, S.P. Sequential ATP hydrolysis by Cdc6 and ORC directs loading of the Mcm2–7 helicase. *Mol. Cell* **21**, 29–39 (2006).
42. Ranjan, A. & Gossen, M. A structural role for ATP in the formation and stability of the human origin recognition complex. *Proc. Natl. Acad. Sci. USA* **103**, 4864–4869 (2006).
43. Clarey *et al.* Nucleotide-dependent conformational changes in the DnaA-like core of the origin-recognition complex. *Nat. Struct. Mol. Biol.* advance online publication 9 July 2006 (doi: 10.1038/nsmb1121).
44. Otwinowski, Z. & Minor, W. Processing of X-ray diffraction data collected in oscillation mode. *Methods Enzymol.* **276**, 472–494 (1997).
45. Read, R.J. Pushing the boundaries of molecular replacement with maximum likelihood. *Acta Crystallogr. D Biol. Crystallogr.* **57**, 1373–1382 (2001).
46. Brunger, A.T. *et al.* Crystallography & NMR system: a new software suite for macromolecular structure determination. *Acta Crystallogr. D Biol. Crystallogr.* **54**, 905–921 (1998).
47. Terwilliger, T.C. Maximum-likelihood density modification. *Acta Crystallogr. D Biol. Crystallogr.* **56**, 965–972 (2000).
48. Jones, T.A., Zou, J.Y., Cowan, S.W. & Kjeldgaard, M. Improved methods for building protein models in electron density maps and the location of errors in these models. *Acta Crystallogr. A* **47**, 110–119 (1991).
49. Lamzin, V.S. & Wilson, K.S. Automated refinement of protein models. *Acta Crystallogr. D Biol. Crystallogr.* **49**, 129–147 (1993).
50. Glaser, F. *et al.* ConSurf: identification of functional regions in proteins by surface-mapping of phylogenetic information. *Bioinformatics* **19**, 163–164 (2003).
51. Nielsen, J.E. *et al.* Improving macromolecular electrostatics calculations. *Protein Eng.* **12**, 657–662 (1999).